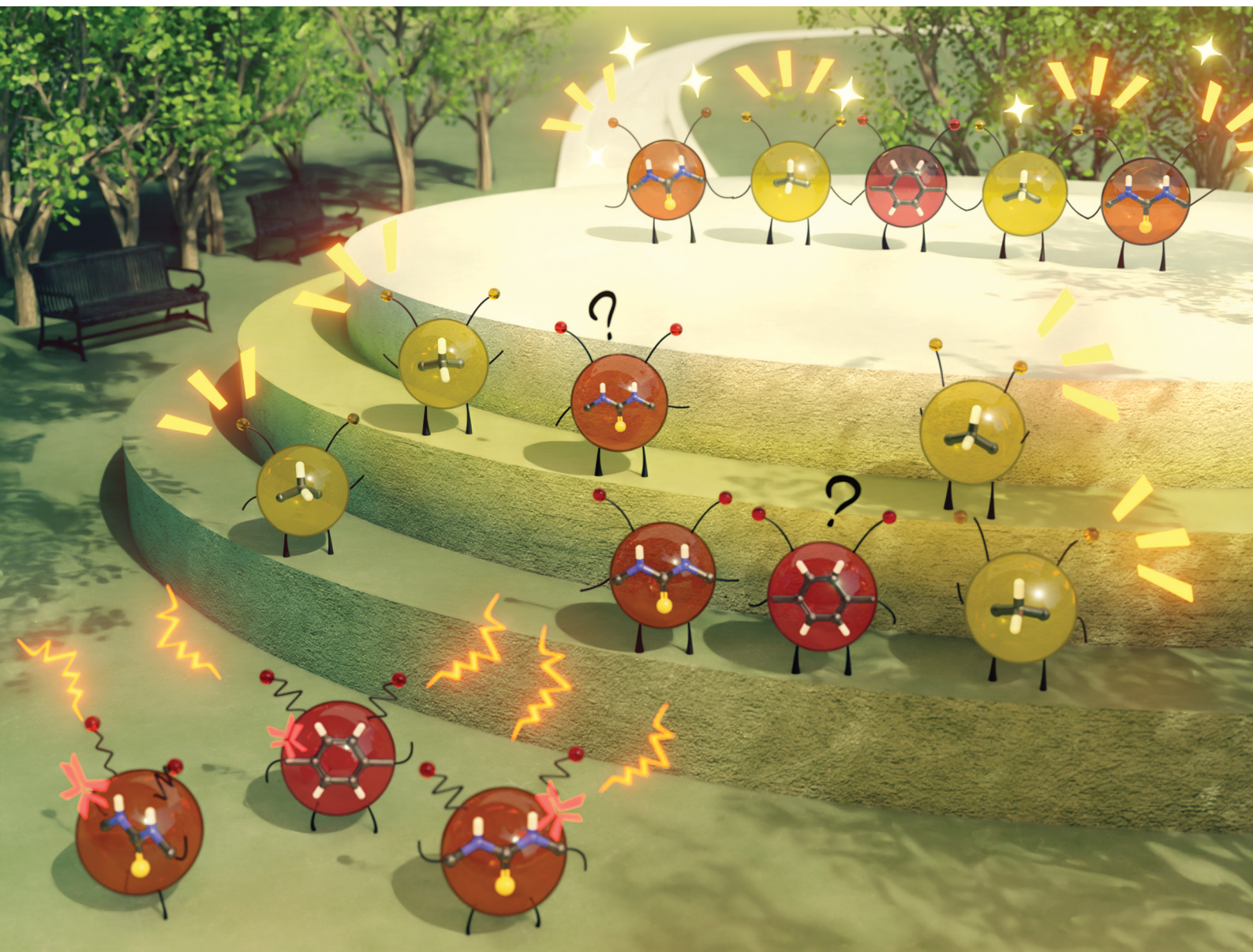


# ChemComm

Chemical Communications

rsc.li/chemcomm



ISSN 1359-7345

**COMMUNICATION**

Kenichi Oyaizu *et al.*

Bleaching effect of high refractive index xylylic poly(thiourea)s with “de-conjugated” polarizable hydrogen bonds


 Cite this: *Chem. Commun.*, 2025, 61, 16002

 Received 4th July 2025,  
 Accepted 9th September 2025

DOI: 10.1039/d5cc03785a

rsc.li/chemcomm

# Bleaching effect of high refractive index xylylic poly(thiourea)s with “de-conjugated” polarizable hydrogen bonds

 Seigo Watanabe,<sup>a</sup> Yoshino Tsunekawa<sup>b</sup> and Kenichi Oyaizu<sup>id</sup>\*<sup>ab</sup>

**Poly(*p*-xylylene thiourea) (pX-PTU) exhibits high visible-light transparency ( $\%T \geq 99$ ), a high refractive index ( $n_D = 1.71$ ), and a reasonable Abbe number ( $\nu_D = 26$ ) owing to “de-conjugated” hydrogen bonds, which inhibit orbital interactions between the polarizable phenylene and thiourea units through sandwiched methylene spacers. Upon blending pX-PTU with all-aromatic poly(thiourea)s, their refractive index increased up to  $n_D = 1.80$ .**

High refractive index polymers (HRIPs) typically exhibit refractive indices (RI) above 1.7 and are essential in various optoelectronic applications, including lighting devices, waveguides, and augmented/mixed reality (AR/MR).<sup>1–5</sup> To date, numerous HRIPs have been developed based on the Lorentz–Lorenz equation, which requires optimizing high polarizability and small molecular volume to achieve the desired RI and transparency at the target wavelength.<sup>2,4</sup> The most common HRIP categories are sulfur-containing polymers, such as poly(phenylene sulfide)s,<sup>4,6–10</sup> sulfur-rich polymers,<sup>3,11–13</sup> and thioacetal-containing polymers.<sup>14,15</sup> In particular, HRIPs with excessive sulfur content or conjugated  $\pi$ -skeletons achieve ultrahigh RI (over 1.8),<sup>11,16,17</sup> but they are colored due to the orbital interactions among  $\pi$ -skeletons and/or sulfur lone pairs (*e.g.*,  $n$ - $\pi$  interactions<sup>18</sup>). To address this empirical dilemma, we previously developed hydrogen-bonding (H-bonding) poly(phenylene sulfide)s to achieve both ultrahigh RI ( $n_D \sim 1.80$ – $1.85$ ) and visible-light transparency.<sup>19,20</sup> The key factor lies in the reduced free volume, which enhances the RI without compromising UV-visible (UV-vis) transparency. We further extended this concept to all-aromatic poly(thiourea)s (PTUs) featuring multiple and polarizable H-bonds, exhibiting better RI ( $n_D \sim 1.7$ – $1.8$ ) and flexibility owing to strengthened PTU networks.<sup>21,22</sup> Also, other researchers have recently reported diverse high-RI PTU structures.<sup>23,24</sup> However, although all-aromatic PTU thin films are

nearly colorless, their transparency remains low ( $\%T \geq 92$ , 1  $\mu\text{m}$  thick) owing to the direct coupling of polarizable thiourea and aromatic rings, which leads to excessive orbital interactions resulting in near-UV absorption and small Abbe numbers ( $\nu_D = 11$ – $18$ ).<sup>21</sup>

In this study, we provide a new concept, termed as “de-conjugated” polarizable H-bonds, to significantly enhance the transparency of high-RI PTUs (Fig. 1). The key design is poly(xylylene thiourea) (X-PTU), which contains a sandwiched methylene spacer that separates polarizable aromatic and thiourea groups, thereby inhibiting orbital interactions. In particular, *p*-substituted X-PTU (**pX-PTU**) exhibited amorphous and thermal properties comparable to those of the all-aromatic PTUs, while displaying improved transparency ( $\%T \geq 99$ ) and a higher Abbe number ( $\nu_D = 26$ ) with its high RI ( $n_D = 1.71$ ) maintained (Fig. 1, right). In addition, **pX-PTU** showed good miscibility with all-aromatic poly(1,3-phenylene-*alt*-1,4-phenylene thiourea) (**mpPh-PTU**), producing simply blended transparent films with an enhanced  $T_g$  and well-balanced optical properties ( $T_g = 164$  °C,  $n_D = 1.80$ ,  $\nu_D = 17$ ). Overall, this study highlights the potential of the “de-conjugated” H-bonding X-PTU and its polymer blends as a rational approach to simultaneously maximize various properties (*e.g.*, RI, Abbe numbers, and transparency) for versatile optoelectronic polymers.

The X-PTUs were synthesized following our previous report,<sup>21</sup> involving the polycondensation of xylylene diamines (XDA) and 1,1-thiocarbonyl diimidazole (Schemes S1 and S2).

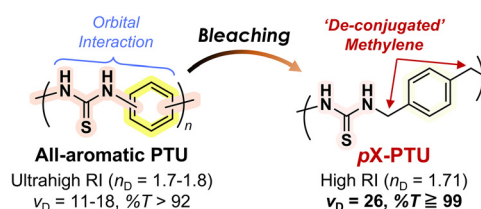


**Fig. 1** The concept of “de-conjugated” polarizable H-bonds: from all-aromatic PTU<sup>21</sup> (left: prior work) to **pX-PTU** (right: this work) to bleach high-RI PTUs.

<sup>a</sup> Research Institute for Science and Engineering, Waseda University, 3-4-1 Okubo, Shinjuku-ku, Tokyo 169-8555, Japan. E-mail: oyaizu@waseda.jp

<sup>b</sup> Department of Applied Chemistry, Waseda University, 3-4-1 Okubo, Shinjuku-ku, Tokyo 169-8555, Japan



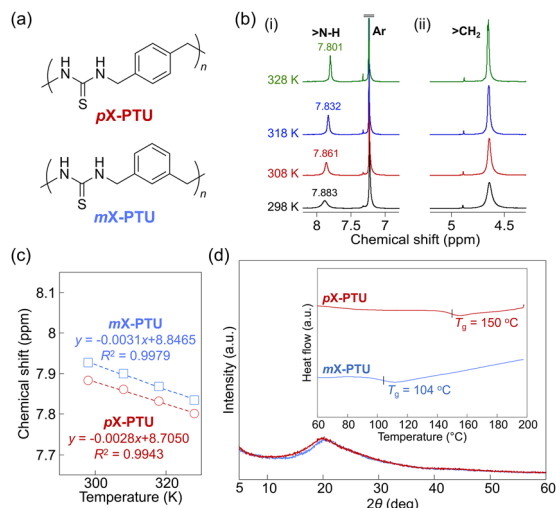


**Fig. 2** Properties of X-PTUs. (a) Chemical structures of *pX*-PTU and *mX*-PTU. (b) <sup>1</sup>H VT-NMR of *pX*-PTU (i) at 8.2–6.8 ppm (>N–H and aromatic signals) and (ii) at 5.2–4.3 ppm (methylene signals). (c) Temperature dependence of >N–H chemical shifts in <sup>1</sup>H VT-NMR. (d) XRD profiles (inset: DSC thermograms at a scan rate of 20 °C min<sup>-1</sup>).

Two *m*- and *p*-substituted PTU isomers (*mX*-PTU and *pX*-PTU) were obtained as high-molecular-weight polymers ( $M_w \sim 10^5$ ), owing to the higher nucleophilicity of XDAs compared with that of all-aromatic diamines (Fig. 2a). The resulting X-PTUs were characterized by <sup>1</sup>H and <sup>13</sup>C NMR spectroscopy, showing signals of thiourea, aromatic, and methylene groups (Fig. S1–S4). The IR spectra indicate two N–H conformations of thiourea ( $\nu_{\text{N–H}}(\text{trans/trans})$ :  $\sim 3270$  cm<sup>-1</sup> and  $2\delta_{\text{N–H}}(\text{cis/trans})$ :  $\sim 3055$  cm<sup>-1</sup>), suggesting the presence of randomized H-bond networks (Fig. S5). Upon increasing the temperature, the <sup>1</sup>H variable-temperature (VT) NMR spectra of the X-PTUs showed an upfield shift exclusively for the H-bonding amino signals (7.93–7.80 ppm) (Fig. 2b and Fig. S6). Notably, *pX*-PTU exhibited lower temperature dependence ( $-2.8 \times 10^{-3}$  ppm K<sup>-1</sup>) than *mX*-PTU ( $-3.1 \times 10^{-3}$  ppm K<sup>-1</sup>) and previously reported phenylene-PTUs ( $< -3.5 \times 10^{-3}$  ppm K<sup>-1</sup>)<sup>21</sup> (Fig. 2c). These results indicate that *pX*-PTU contains stronger and more high-temperature-resistant intermolecular H-bond network.

Regarding the crystalline properties, the X-ray diffraction (XRD) profiles indicate an amorphous nature of X-PTUs, which can be attributed to the zig-zag H-bonds of the thiourea arrays (Fig. 2d). *X*-PTU exhibited good thermostability, with both an adequate  $T_g$  ( $> 100$  °C) and a high pyrolysis temperature ( $T_{d5} \sim 240$ – $250$  °C), significantly surpassing those of phenylene-PTUs ( $T_g \sim 150$  °C,  $T_{d5} \sim 180$  °C)<sup>21</sup> (Fig. 2d inset, Fig. S7). This superior thermostability can be attributed to the deconjugated X-PTU structure containing methylene spacers, which enhance the bond stability (dissociation energy) of the C–N bonds, similar to the effect observed in aromatic/xylylic poly(dithiourethane)s.<sup>25</sup> Among the X-PTUs, *pX*-PTU showed a significantly higher  $T_g$  (150 °C) than *mX*-PTU ( $T_g = 104$  °C), owing to the stronger and more temperature-resistant interchain H-bonds in the linear-shaped *p*-phenylene skeleton compared with the bent-shaped *m*-phenylene unit.

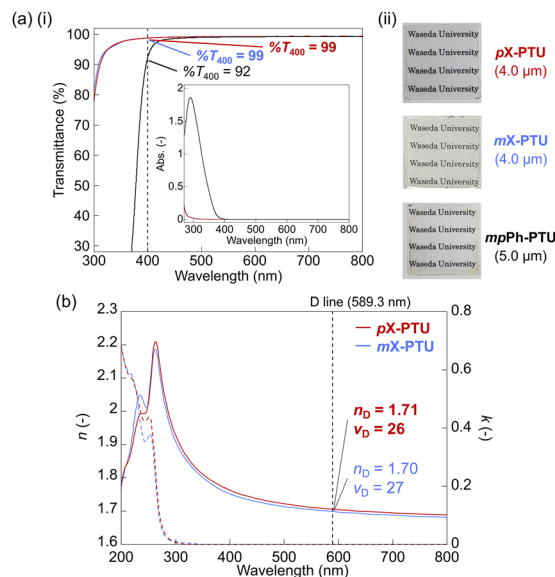


**Fig. 3** Optical properties of X-PTUs. (a) (i) Normalized UV-vis spectra for the films (thickness: 1 μm) of X-PTUs and *mpPh*-PTU (inset: UV-vis absorbance spectra of 0.1 mM solution in DMF). (ii) Photographs of PTU thin films on glass substrates and their thickness. (b) RI spectra: *n* (solid line) and *k* (dotted line).

Their optical properties were investigated to confirm the introduction effect of “de-conjugated” H-bonds (Fig. 3). The solution UV-vis spectra displayed that the X-PTUs exhibit superior visible-light transparency compared with *mpPh*-PTU, accompanied by a blue shift in near-UV absorption (Fig. 3a inset). This behavior can be attributed to the absence of orbital interactions between the lone pairs/ $\pi$ -electrons of the thioureas and phenylene rings upon the introduction of methylene spacers. To gain molecular-level insight, density functional theory (DFT) calculations were conducted on the model compounds of each polymer (Fig. S8). The orbital geometries of the phenylene-PTU models exhibited a widely distributed highest occupied molecular orbital (HOMO), which strongly overlapped with the lowest unoccupied molecular orbital (LUMO). In contrast, the X-PTU model showed a narrower distribution of continuous HOMO orbitals and less HOMO–LUMO geometry overlap. The estimated UV-vis spectra by time-dependent (TD) DFT calculations reproduced a pronounced blue shift in the near-UV absorption for the X-PTU models (Fig. S9). Therefore, the effect of “de-conjugated” methylene spacers in X-PTUs can be rationalized as the suppression of orbital interactions between thioureas and phenylene rings.

X-PTU thin films were also prepared *via* drop-casting or spin-coating, exhibiting colorless and visually transparent features (Fig. 3a), and the *pX*-PTU film displayed a fluorescence emission under UV irradiation (Fig. S10), as observed in typical PTUs.<sup>26</sup> Their UV-vis spectra display higher near-UV-vis transparency ( $\%T \geq 99$ ) than those of aromatic PTUs, owing to the bleaching effect in the X-PTUs (Fig. 3a(i) and Fig. S11). Following the introduction of methylene spacers, the X-PTUs exhibited lower RI ( $n_D = 1.71$  (*pX*-PTU) and 1.70 (*mX*-PTU)) than previously reported phenylene-PTUs ( $n_D \sim 1.8$ )<sup>21</sup> because of the



decrease in the unit polarizability (Fig. 3b). However, their RI remained within the range of typical HRIPs,<sup>2,4</sup> while the Abbe numbers were markedly improved ( $\nu_D = 26$  (**pX-PTU**) and 27 (**mX-PTU**)) compared with those of the reported phenylene-PTUs ( $\nu_D \sim 11$ –15)<sup>21</sup> and dimethyl-substituted PPS with a similar RI ( $n_D = 1.69$ ,  $\nu_D = 18$ ).<sup>27</sup> These trends follow the classical Kramers–Kronig relationship,<sup>28</sup> which explains that suppressing the near-UV absorption in X-PTUs results in a higher  $\nu_D$ . Furthermore, despite the low UV stability of aromatic PTUs ascribed to the presence of reactive C=S bonds<sup>29</sup> that induced lower transparency and RI (Fig. S12 and S13), the optical properties of **pX-PTU** were less deteriorated after the UV treatment than those for **mpPh-PTU**, thanks to the “de-conjugated” xylylene unit with less orbital interactions. In addition, there has been minimal change in RI and transparency of **pX-PTU** after the high-temperature or humid exposure (difference of % $T_{400} \sim 1\%$ ,  $n_D \sim \pm 0.01$ ) (Fig. S14–S17), attributed to the high hydrophobicity and rigidity ( $T_g$ ) of the aromatic main chain and the relatively hydrophobic H-bond properties<sup>30</sup> of the thiourea moieties to prevent H-bond network destruction. Finally, the **pX-PTU** film displayed higher stress (17.2 MPa) and smaller strain (0.64%) upon fracture than the previous aromatic PTU (12 MPa, 2.4%)<sup>22</sup> (Fig. S18), suggesting higher mechanical robustness due to the stronger H-bond nature of X-PTUs (Fig. 2c: *vide supra*).

In light of the high-RI yet transparent optical properties of X-PTU, we further adjusted the thermostability and RI while maintaining high transparency by applying a blending strategy with different PTUs.<sup>31</sup> We selected **mpPh-PTU** as a blending counterpart because of its higher  $T_g$  (175 °C) and RI ( $n_D = 1.81$ ). Each PTU was blended by precipitating the DMF solution into methanol, yielding **pX-PTU/mpPh-PTU** blends with **pX-PTU** molar ratios of  $x_{\text{pX-PTU}} = 0.72, 0.49, \text{ and } 0.24$  (Fig. S19–S21). Their DSC thermograms display a single  $T_g$  that shifts to higher temperature as  $x_{\text{pX-PTU}}$  decreases (Fig. 4a), indicating good miscibility between each PTU with 10–20 nm scale homogeneity.<sup>32</sup> To further elucidate their miscibility on a smaller scale, we conducted cross-polarization/magic angle spinning (CP/MAS) <sup>13</sup>C NMR on the **pX-PTU/mpPh-PTU** blends (Fig. S23–S27). In short, the <sup>1</sup>H spin–lattice relaxation time ( $T_{1\rho}$ ) was determined from two areas, aromatic (*ca.* 150–100 ppm) and

methylene (*ca.* 55–35 ppm) signals, for each composition (Fig. S28). While those  $T_{1\rho}$ s did not match perfectly, they shifted proportionally with  $x_{\text{pX-PTU}}$ , confirming interdomain interactions between **pX-PTU** and **mpPh-PTU** in the blended matrices (Fig. 4b and Table S1). Therefore, although those PTUs were phase-separated on a 3–4 nm scale detectable by CP/MAS NMR measurements, they are miscible on a scale below 20 nm, as indicated by the  $T_g$  shifts observed in the DSC results.

The drop-cast **pX-PTU/mpPh-PTU** blend films were visibly transparent and exhibited no aggregation, further confirming the good miscibility of the PTUs (Fig. 5a inset). The UV-vis spectra of the blend films showed good transparency (94–96% $T$  for 1  $\mu\text{m}$  thickness), falling between the values of the individual PTUs regardless of the film thickness (Fig. 5a, Table S2, and Fig. S29–S31). These results demonstrated the bleaching effect with improved near-UV transparency upon increasing  $x_{\text{pX-PTU}}$ . Their ATR-IR spectra showed a consistent peak shift of the H-bonded N–H vibration modes ( $\nu_{\text{N-H}}$  and  $2\delta_{\text{N-H}}$ ) (Fig. S32), indicating the presence of homogeneous H-bond networks even in the blended states without any macroscopic phase separation.

The RI spectra also followed consistent shifts in  $n_D$  and  $\nu_D$  corresponding to the blending ratio (Fig. 5b). In short, the **pX-PTU/mpPh-PTU** blend with higher  $x_{\text{pX-PTU}}$  exhibited a lower RI and higher  $\nu_D$  across the entire visible-light region, aligning well with the empirical RI–Abbe trade-off relationship<sup>33</sup> (Fig. 5c). The extinction coefficient ( $k$ , the imaginary part of the complex RI) also decreased with higher  $x_{\text{pX-PTU}}$ , demonstrating the bleaching effect upon **pX-PTU** introduction (Fig. S33). Summarizing the above, **pX-PTU** was miscible with aromatic PTU on a 10–20 nm scale, and their polymer blends produced transparent films with enhanced thermostability and RI. In particular, entry 3 ( $x_{\text{pX-PTU}} = 0.24$ ; Table S2) showed the best balance of thermal and optical

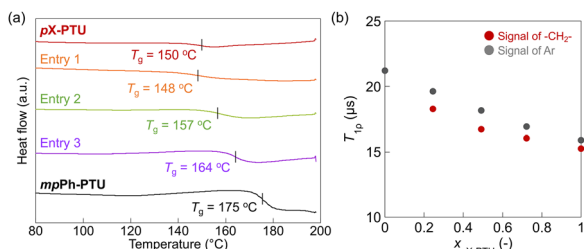


Fig. 4 Miscibility studies of **pX-PTU** and **mpPh-PTU**. (a) DSC thermograms of the blends (2nd heating, scanning rate: 20 °C min<sup>-1</sup>). (b) Relationship between <sup>1</sup>H spin–lattice relaxation time ( $T_{1\rho}$ ) of the blends measured by solid-state CP-MAS <sup>13</sup>C NMR and the molar ratio of **pX-PTU** ( $x_{\text{pX-PTU}}$ ).

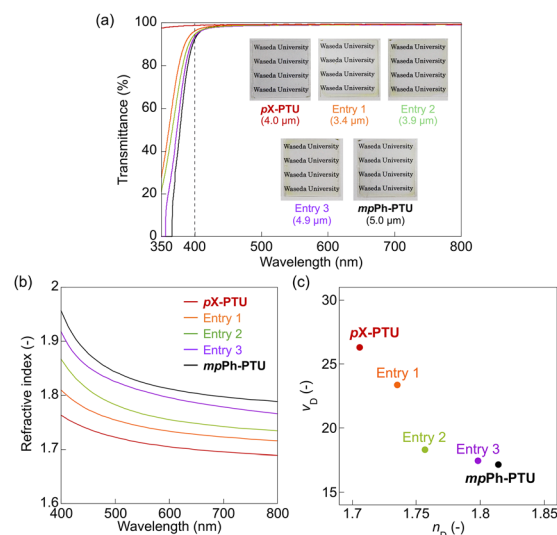


Fig. 5 Optical properties of the films of the **pX-PTU/mpPh-PTU** blends. (a) Normalized UV-vis spectra (film thickness: 1  $\mu\text{m}$ ) (inset: photographs and thickness of the films). (b) RI spectra in the visible-light region (for the overall spectra, see Fig. S32). (c)  $n_D$  versus  $\nu_D$ .



properties among the PTU family, exhibiting a high  $T_g$  (164 °C) and ultrahigh RI ( $n_D = 1.80$ ), while simultaneously achieving a reasonable Abbe number ( $\nu_D = 17$ ) and visible light transparency (94%T, 1  $\mu\text{m}$  thickness).

In summary, we demonstrated the X-PTU family as an HRIP substructure with unprecedented near-UV-vis transparency and Abbe numbers (e.g., **pX-PTU**:  $n_D = 1.71$ ,  $\nu_D = 26$ ). The key molecular design lies in the “de-conjugated” H-bonds, which involves separating the polarizable aromatic and thiourea moieties with sandwiched methylene spacers to inhibit their orbital interactions while maintaining high polarizability and H-bond density. In particular, **pX-PTU** exhibited adequate thermostability ( $T_g = 150$  °C) and good miscibility with **mpPh-PTU** on a 10–20 nm scale, and their blended films demonstrated adjustable thermal and optical properties. To our knowledge, this study is the first to demonstrate how orbital interactions in an HRIP bearing polarizable H-bonds affect the overall optical properties. Furthermore, miscible polymer blending is verified as a simple strategy to adjust the thermal and optical properties. Expanding this concept to diverse polarizable H-bond containing HRIP skeletons (e.g., poly(thioamide)<sup>23,34</sup> and poly(sulfamide)<sup>35</sup>) leads to the further design of optical polymers surpassing the empirical RI–Abbe trade-off limit.

This work was partially supported by Grants-in-Aid for Scientific Research (No. 21H04695, 22K18335, and 25K18083) from MEXT, Japan, the Satomi Scholarship Foundation, and ENEOS Tonen General Research/Development Encouragement and Scholarship Foundation.

## Conflicts of interest

There are no conflicts to declare.

## Data availability

The data supporting this article have been included as part of the SI. Supplementary information: Experimental and synthetic procedures, characterization data, computational calculation, solid-state NMR results, and additional properties for the blends. See DOI: <https://doi.org/10.1039/d5cc03785a>.

## Notes and references

- J.-G. Liu and M. Ueda, *J. Mater. Chem.*, 2009, **19**, 8907–8919.
- T. Higashihara and M. Ueda, *Macromolecules*, 2015, **48**, 1915–1929.
- T. S. Kleine, R. S. Glass, D. L. Lichtenberger, M. E. Mackay, K. Char, R. A. Norwood and J. Pyun, *ACS Macro Lett.*, 2020, **9**, 245–259.
- S. Watanabe and K. Oyaizu, *Bull. Chem. Soc. Jpn.*, 2023, **96**, 1108–1128.
- A. Nishant, K.-J. Kim, S. A. Showghi, R. Himmelhuber, T. S. Kleine, T. Lee, J. Pyun and R. A. Norwood, *Adv. Opt. Mater.*, 2022, **10**, 2200176.
- Y. Suzuki, K. Murakami, S. Ando, T. Higashihara and M. Ueda, *J. Mater. Chem.*, 2011, **21**, 15727–15731.
- K. Nakabayashi, T. Imai, M.-C. Fu, S. Ando, T. Higashihara and M. Ueda, *Macromolecules*, 2016, **49**, 5849–5856.
- M.-C. Fu, Y. Murakami, M. Ueda, S. Ando and T. Higashihara, *J. Polym. Sci., Part A: Polym. Chem.*, 2018, **56**, 724–731.
- S. Watanabe, Y. Tsunekawa, T. Takayama and K. Oyaizu, *Macromolecules*, 2024, **57**, 2897–2904.
- S. Watanabe, Z. An, H. Nishio, Y. Tsunekawa and K. Oyaizu, *J. Mater. Chem. C*, 2025, **13**, 7933–7942.
- J. J. Griebel, S. Namnabat, E. T. Kim, R. Himmelhuber, D. H. Moronta, W. J. Chung, A. G. Simmonds, K.-J. Kim, J. van der Laan, N. A. Nguyen, E. L. Dereniak, M. E. Mackay, K. Char, R. S. Glass, R. A. Norwood and J. Pyun, *Adv. Mater.*, 2014, **26**, 3014–3018.
- D. H. Kim, W. Jang, K. Choi, J. S. Choi, J. Pyun, J. Lim, K. Char and S. G. Im, *Sci. Adv.*, 2020, **6**, eabb5320.
- K.-S. Kang, C. Olikagu, T. Lee, J. Bao, J. Molineux, L. N. Holmen, K. P. Martin, K.-J. Kim, K. H. Kim, J. Bang, V. K. Kumirov, R. S. Glass, R. A. Norwood, J. T. Njardarson and J. Pyun, *J. Am. Chem. Soc.*, 2022, **144**, 23044–23052.
- S. Watanabe, T. Yano, Z. An and K. Oyaizu, *ChemSusChem*, 2025, **18**, e202401609.
- J.-Z. Zhao, T.-J. Yue, B.-H. Ren, Y.-X. Ma, X.-B. Lu and W.-M. Ren, *J. Am. Chem. Soc.*, 2025, **147**, 19762–19769.
- X. Wu, J. He, R. Hu and B. Z. Tang, *J. Am. Chem. Soc.*, 2021, **143**, 15723–15731.
- M. Lee, Y. Oh, J. Yu, S. G. Jang, H. Yeo, J.-J. Park and N.-H. You, *Nat. Commun.*, 2023, **14**, 2866.
- A. Fukazawa, Y. Toda, M. Hayakawa, A. Sekioka, H. Ishii, T. Okamoto, J. Takeya, Y. Hijikata and S. Yamaguchi, *Chem. – Eur. J.*, 2018, **24**, 11503–11510.
- S. Watanabe and K. Oyaizu, *Macromolecules*, 2022, **55**, 2252–2259.
- S. Watanabe, H. Nishio, T. Takayama and K. Oyaizu, *ACS Appl. Polym. Mater.*, 2023, **5**, 2307–2311.
- S. Watanabe, L. M. Cavinato, V. Calvi, R. van Rijn, R. D. Costa and K. Oyaizu, *Adv. Funct. Mater.*, 2024, **34**, 2404433.
- S. Watanabe, Y. Tsunekawa and K. Oyaizu, *Macromol. Chem. Phys.*, 2025, **226**, 2400456.
- Y. Huang, R. Hu and B. Z. Tang, *Macromolecules*, 2024, **57**, 6568–6576.
- Y. Yu, W. Chen, R. Hu and B. Z. Tang, *Polym. Chem.*, 2025, **16**, 1509–1518.
- Y. Yoshida and T. Endo, *J. Polym. Sci., Part A: Polym. Chem.*, 2018, **56**, 2255–2262.
- J. Zhang, F. Ye, J.-L. Huo, J.-W. Peng, R.-R. Hu and B. Z. Tang, *Chin. J. Polym. Sci.*, 2023, **41**, 1563–1576.
- S. Watanabe, T. Takayama, H. Nishio, K. Matsushima, Y. Tanaka, S. Saito, Y. Sun and K. Oyaizu, *Polym. Chem.*, 2022, **13**, 1705–1711.
- M. Fox, *Optical Properties of Solids*, OUP, Oxford, 2001, vol. 70.
- S. Yoo, H. Park, Y. S. Kim, J. C. Won, D.-G. Kim and Y. H. Kim, *J. Mater. Chem. C*, 2021, **9**, 77–81.
- K. Kikkawa, Y. Sumiya, K. Okazawa, K. Yoshizawa, Y. Itoh and T. Aida, *J. Am. Chem. Soc.*, 2024, **146**, 21168–21175.
- Y. Fujisawa, Y. Nan, A. Asano, Y. Yanagisawa, K. Yano, Y. Itoh and T. Aida, *Angew. Chem., Int. Ed.*, 2023, **62**, e202214444.
- A. Asano and T. Kurotu, *J. Mol. Struct.*, 1998, **441**, 129–135.
- S. Watanabe, T. Takayama and K. Oyaizu, *ACS Polym. Au*, 2022, **2**, 458–466.
- Y. Hu, L. Zhang, Z. Wang, R. Hu and B. Z. Tang, *Polym. Chem.*, 2023, **14**, 2617–2623.
- J. W. Wu, R. W. Kulow, M. J. Redding, A. J. Fine, S. M. Grayson and Q. Michaudel, *ACS Polym. Au*, 2023, **3**, 259–266.

